ELSEVIER

Journal of Applied Geophysics 42 (1999) 243–260

JOURNAL OF APPLIED GEOPHYSICS

Multifocusing homeomorphic imaging Part 2. Multifold data set and multifocusing

Boris Gelchinsky [a,*], Alexander Berkovitch [a], Shmariahu Keydar [b]

[a] *Tel Aviv University, Department of Geophysics and Planetary Sciences, University Campus, Ramat-Aviv, Tel Aviv 69978, Israel*

[b] *The Geophysical Institute of Israel, P.O. Box 182, Lod 71100, Israel*

Abstract

In this paper, we continue the construction of the multifocusing technique which is devoted to correlation and stacking of body wavefields, and determination of their kinematic attributes and amplitudes. In the first part of the work (Gelchinsky et al., 2000a), we obtain the local time correction formula for a pair of traces (the first is fixed and the second is any trace recorded in the vicinity of the first). The formula contains certain parameters, common for all traces and belonging to the so-called spherical vicinity and a pair of dual curvatures of two cross-sections of a ray tube surrounding the central ray and associated with the considered pair of traces. It was proved that an infinite family of the dual curvatures associated with the fixed central ray can be parameterized. The parameterization formulae contain, as parameters, the dual curvatures of the pair of fundamental ray tubes. The formula variable determining each ray tube is measured along the central ray. The parameterization formulae are only determined on the central ray. In order to use the formulae for the time correction, it is necessary to continue them in the vicinity of the central ray. A main idea behind this continuation is the establishment of a unique correspondence between each pair of traces consisting of the fixed central trace and another current trace recorded in its vicinity by a multifold acquisition system and a certain ray tube surrounding a central ray. More specifically, the establishment of this correlation means finding a formula for the parameterization variable for any trace recorded in the vicinity of a central trace. If the variable is known, then the values of the dual curvatures for a specific ray tube can be calculated using the parameterization formulae. In the first stage, the equation establishing the functional dependence between offsets of source and receiver is derived. This equation contains, as a parameter, the parameterization variable mentioned above. The equation derived is applied to the determination of special configurations of source–receiver pairs situated on two straight lines in the vertical plane. In the next stage, the solution of the equation with respect to the parameterization variable is found. The formula obtained facilitates calculation of the value of the variable for any trace, for which offsets of source and receiver are given and the parameters of the ray tube family are fixed. These parameters are the angles of departure and entry, the pair of two dual curvatures for two fixed fundamental ray tubes, if configuration with a nonzero offset central ray is considered. In the case of a zero offset normal central ray, the parameters are the angle of entry, and the Common Evolute Element (CEE) and Common Reflecting Element (CRE) curvatures. We also present a kinematic analysis of the obtained formulae. In particular, we show that the parameterization variable has a geometrical meaning as a focusing parameter. In order to make the consideration of the vicinity of a central ray more applicable, the Multifocusing Stacking Chart is proposed. It is shown that all traces recorded by an arbitrary acquisition system could be time-corrected. The number of traces corrected by multifocusing is the product of a multifolding degree and the number of traces in the CSP seismogram. Thus, in the case of modern acquisition systems, the number of stacked traces may vary from many hundreds to

* Corresponding author. Fax: +972-3-6409282; e-mail: shemer@gii.co.il

0926-9851/99/$ - see front matter
PII: S0926-9851(99)00039-7

dozens of thousands. The flow chart of multifocusing correlation and the stacking algorithm is presented and discussed. Its output is a set of time sections presenting optimally stacked wavefields, angle of entry (anglegram), CEE and CRE radii (CEE and CRE radiusgrams) and maximum semblance (semblancegram) as 2D functions of coordinates of central traces and zero times. Thus, the procedure of optimal correlation and stack facilitates transformation of a set of hundreds or thousands of traces recorded near each central trace into an ensemble of time sections of different types presenting kinematics and averaged attributes of wavefields.

Keywords: Multifocusing; Traces; Wavefields

1. Parameterization of a family of ray tubes surrounding a fixed ray

In the first part of the work, the expressions parameterizing a family of wavefront curvatures given on a fixed ray were derived. In this section, the formulae are continued in the vicinity of the ray, determining a family of surrounding ray tubes.

We start by finding an equation establishing the relation between increments of coordinates of sources and receivers connected by rays. Assigning

(a) coordinates of source and receiver by x^- and x^+, connected by the ray A^-CA^+ (Fig. 1),

(b) related spreadings by Q^- and Q^+ and

(c) wavefront square elements (arc's length in 2D case) by $\mathrm{d}\sigma^-$ and $\mathrm{d}\sigma^+$,

we can write the equations

$$\frac{\mathrm{d}x^-}{\mathrm{d}\sigma^-} = \frac{1}{\cos\beta^-}, \quad \frac{\mathrm{d}x^+}{d\sigma^+} = \frac{1}{\cos\beta^+} \tag{1}$$

obviously from a geometrical point of view (Fig. 1).

Using expression (1) and the well-known formula

$$\mathrm{d}\sigma^-/\mathrm{d}\sigma^+ = (Q^-)/(Q^+), \tag{2}$$

we can obtain the equation

$$\frac{\mathrm{d}x^-}{\mathrm{d}x^+} = \frac{Q^-\cos\beta^+}{Q^+\cos\beta^-}. \tag{3}$$

We can now introduce the normalization

$$Q^+ \equiv Q(x^+) = 1 \tag{4}$$

of the spreading Q^+ for all points $A^+(x^+)$, belonging to some vicinity of the central end point $A_0^+(x_0^+)$. Using the relations (14) and (18) from Part 1 of the work and the normalization (4), the formulae

$$Q^+ = a + b = 1, \; Q^- = a - b = 1 - 2b \tag{5}$$

are found. The solution of the first equations from Eq. (5) is

$$a = 1 - b, \; \gamma = b/a = b/(1-b). \tag{6}$$

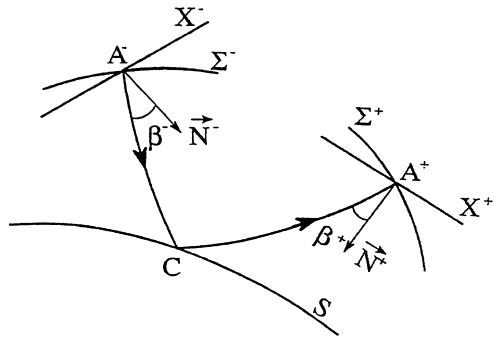

Fig. 1. Disposition of source and receiver lines, reflector and the central path. S is the reflector, X^- (X^+) is the source (receiver) line, β^- (β^+) is the angle of departure (arrival), Σ^- (Σ^+) is the fictitious front leaving (arriving) the source (receiver) point A^- (A^+).

After substitution of the values of Q^+ and Q^- from formulae (5) in Eq. (3), we find the basic equation

$$\frac{\mathrm{d}x^-}{\mathrm{d}x^+} = (1-2b)\frac{\cos\beta^+}{\cos\beta^-}. \tag{7}$$

This differential equation can be used for determination of a functional connection between corresponding offsets $\Delta x_i^+ = x_i^+ - x_0^+$ and $\Delta x_j^- = x_j^- - x_0^-$ in proximity to the end points of the central ray $A_0^- C_0 A_0^+$.

Expanding the right-hand side of the equation in the Taylor series and preserving the first two terms, we obtain, after certain simple manipulations, the relation

$$\Delta x_j^- = (1-2b)(\cos\beta_0^+/\cos\beta_0^-)\left[\Delta x_i^+ - 2\alpha(\Delta x_i^+)^2\right], \tag{8}$$

where

$$2\alpha = -\left(\frac{\cos\beta_0^-}{\cos\beta_0^+}\right)\frac{\partial}{\partial x^+}\left(\frac{\cos\beta^+}{\cos\beta^-}\right). \tag{9}$$

In the Appendix, the following expression

$$2\alpha = -\frac{\sin\beta_0^+\cos\beta_0^-\left[(1-b)k_e^+ + bk_a^+\right] + \sin\beta_0^-\cos\beta_0^+\left[(1-b)k_e^- - bk_a^-\right]}{\cos\beta_0^-}. \tag{10}$$

is derived.

Thus, we find expression (8) with the coefficient α (Eq. (10)) determining an offset Δx_i^-, corresponding to a chosen offset Δx_i^+. The parameters β_0^υ, k_e^υ and k_a^υ ($\upsilon = +$ or $-$) for the central ray and coefficient b are fixed. If the value of b is the same for all selected pairs (Δx_i^+, Δx_i^-), then the distribution of source–receiver pairs satisfies the first generalization principle of the HI mapping formulated above (Gelchinsky and Keydar, 1993) with the two ray congruencies having orthogonal fronts. Calculating the curvatures k_γ^+ and k_γ^- (Eq. (20)) from Part 1, one can find a time correction $\Delta\tau_{ij}$ according to the formulae (9)–(11) from Part 1.

However, the technique described is hardly practical except for a few special cases like such as the CSP and CEE configuration. The values of Δx_i, calculated according to Eq. (8) and used through acquisition of seismic data, will, as a rule, be different. Thus, interpolation of the time delay calculations will be required. Moreover, it is more important to find a method to select the value of the parameter b or γ, which ensures complete use of all traces in a stack procedure, recorded in the ''spherical vicinity'' of the fixed ray (trace), is very difficult. In order to find this ''secure way'', the following method is proposed.

The formulae determining the value b_{ij} of the parameter b for each pair of offsets Δx_i^+ and Δx_j^- used by data acquisition are found. This is accomplished by solving a kind of an inverse problem: to determine the value b_{ij}, if the parameters of a ray tube family $\sin\beta_0^{\upsilon}$, k_e^{υ} and (k_a^{υ}) ($\upsilon = +$ or $-$) are fixed and offsets Δx_i^+ and Δx_j^- are chosen.

The problem is solved with the help of the equality

$$1 - 2\alpha\Delta x_i^+ = \left[1 - \left(2\alpha\Delta x_i^+\right)^2\right]/\left(1 + 2\alpha\Delta x_i^+\right). \tag{11}$$

Neglecting the second term in the right-hand side of Eq. (11) under the condition

$$\left(2\alpha\Delta x_i^+\right)^2 \ll 1, \tag{12}$$

and substituting the remaining first term into the relation (8), we obtain the transformed formula

$$\Delta x_j^- = \frac{\left(1 - 2b_{ij}\right)\cos\beta_0^+\Delta x_i^+}{\cos\beta_0^-\left(1 + 2\alpha_{ij}\Delta x_i^+\right)} \tag{13}$$

for a source (receive) distribution, if locations of receivers (sources) are known.

Solving the last equation with respect to b_{ij}, we find

$$b_{ij} = \left(\cos\beta_0^+\Delta x_i^+ - \cos\beta_0^-\Delta x_j^- - 2\alpha_{ij}\cos\beta_0^-\Delta x_i^+\Delta x_j^-\right)/2\cos\beta_0^+\Delta x_0^+. \tag{14}$$

Substituting the value α_{ij} from Eq. (10) into the formula (14), we obtain

$$b_{ij} = \frac{\cos\beta_0^+\Delta x_i^+ - \cos\beta_0^-\Delta x_j^- + \left(\sin\beta_0^+\cos\beta_0^-k_e^+ + \sin\beta_0^-\cos\beta_0^+k_e^-\right)\Delta x_i^+\Delta x_j^-}{2\cos\beta_0^-\Delta x_i^+ + \left[\sin\beta_0^+\cos\beta_0^-\left(k_e^+ - k_a^+\right) + \sin\beta_0^-\cos\beta_0^+\left(k_e^- + k_a^-\right)\right]\Delta x_i^+\Delta x_j^-}. \tag{15}$$

Now the time correction $\Delta\tau_{ij}$ could be determined without interpolation. The coefficient b_{ij} (and γ_{ij}) is calculated according to Eq. (15) for each pair Δx_i^+ and Δx_j^-. The dual curvatures k_{ij}^+ and k_{ij}^- are determined with the help of formulae (20) (in Part 1) and finally the corresponding time delay $\Delta\tau_{ij}$ is found from the expressions (9)–(11) from Part 1.

If the time correction procedure is used by processing multifold seismic data, then all traces belonging to $(m \times n)$ vicinity of the fixed central ray could be taken into account by changing the corrected pairs Δx_i^+ and Δx_j^- $(i = 1,\ldots,m,\ j = 1,\ldots,n)$.

2. The ray tube parameterization for reflection shooting

In this section, we consider the formulae for the parameterization of the family of ray tubes and related types of source–receiver configurations, when the end points A_0^+ and A_0^- coincide and a normally reflected ray is chosen. In this special case, which is most important for reflection shooting, the obtained equations take much simpler forms and certain direct conclusions can be made.

As it was found in Section 1, the boundary conditions for angles of departure (entry) and dual curvatures can be written in the forms (37) and (38) from Part 1. Taking into account these conditions, we transform the general expression (15) for the coefficient b_{ij} to the much simpler equation

$$b_{ij} = \frac{\Delta x_i^+ - \Delta x_j^-}{2\left(\Delta x_i^+ - \sin\beta_0 k_{\mathrm{CRE}} \Delta x_i^+ \Delta x_j^-\right)}. \tag{16}$$

A value γ_{ij} of the parameter γ in formula (6) is determined by

$$\gamma_{ij} = \frac{\Delta x_i^+ - \Delta x_j^-}{\Delta x_i^+ + \Delta x_j^- - 2\sin\beta_0 k_{\mathrm{CRE}} \Delta x_i^+ \Delta x_j^-}. \tag{17}$$

After substituting the γ_{ij} from the last formula into the expressions (39) from Part 1, we find the following relationships for the dual curvatures

$$k_{ij}^+ = \frac{(k_{\mathrm{CEE}} + k_{\mathrm{CRE}})\Delta x_i^+ + (k_{\mathrm{CEE}} - k_{\mathrm{CRE}})\Delta x_j^- - 2\sin\beta_0 k_{\mathrm{CEE}} k_{\mathrm{CRE}} \Delta x_i^+ \Delta x_j^-}{2\Delta x_i^+\left(1 - \sin\beta_0 k_{\mathrm{CRE}} \Delta x_j^-\right)} \tag{18}$$

and

$$k_{ij}^- = -\frac{(k_{\mathrm{CEE}} - k_{\mathrm{CRE}})\Delta x_i^+ + (k_{\mathrm{CEE}} + k_{\mathrm{CRE}})\Delta x_j^- - 2\sin\beta_0 k_{\mathrm{CEE}} k_{\mathrm{CRE}} \Delta x_i^+ \Delta x_j^-}{2\Delta x_j^-\left(1 - \sin\beta_0 k_{\mathrm{CRE}} \Delta x_i^+\right)}. \tag{19}$$

The expression (10) for the coefficient α determining the receivers' (sources') distribution, if the locations of the sources (receivers) are given, is also simplified to the form

$$\alpha = \sin\beta_0 k_{\mathrm{CRE}} b. \tag{20}$$

In this case, the expression (13) for the receiver distribution takes the form

$$\Delta x_j^- = (1 - 2b)\Delta x_i^+ / (1 + 2\sin\beta_0 k_{\mathrm{CRE}} b \Delta x_i^+). \tag{21}$$

If the value of the coefficient b is chosen according to the condition $b = 1$, than the last formula goes to the Common Reflecting Element (CRE) distribution

$$\Delta x_j^- = -\Delta x_i^+ / (1 + 2\sin\beta_0 k_{\mathrm{CRE}} \Delta x_i^+). \tag{22}$$

This expression could be obtained from the formula (5) in Part 1 for the binomial distribution, using the equality (11) under the condition (12).

If $b = 0$, then Eq. (21) is degenerated to the simple condition

$$\Delta x_i^+ = \Delta x_j^-, \tag{23}$$

which can be satisfied if only the equality

$$x_j^- = x_i^+ \tag{24}$$

takes place. It is the zero-offset CEE source–receiver configuration.

These two special (CRE and CEE) distributions could be generalized for situation where the end points of the ray do not coincide. They correspond to the conditions: $b = 0$ (CEE) and $b = 1$ (CRE).

If $b = 0$, then the expressions (13) and (10) take the forms

$$\Delta x_i^- = \frac{\cos\beta_0^+ \Delta x_i^+}{\cos\beta_0^- \left(1 + 2\alpha_{\mathrm{GCEE}} \Delta x_i^+\right)}, \tag{25}$$

where

$$2\alpha_{\mathrm{GCEE}} = -\left(\sin\beta_0^+ \cos\beta_0^- k_e^+ + \sin\beta_0^- \cos\beta_0^+ k_e^-\right)/\cos\beta_0^- . \tag{26}$$

The Generalized Common Reflecting Element (GCRE) configuration is determined by

$$\Delta x_i^- = -\frac{\cos\beta_0^+ \Delta x_i^+}{\cos\beta_0^- \left(1 + 2\alpha_{\mathrm{GCRE}} \Delta x_i^+\right)} \tag{27}$$

with the factor α given by

$$2\alpha_{\mathrm{GCRE}} = \left(\sin\beta_0^- \cos\beta_0^+ k_a^- - \sin\beta_0^+ \cos\beta_0^- k_a^+\right)/\cos\beta_0^- . \tag{28}$$

3. Combined CMP and CO approximation of NMO for small offsets

This section is devoted to modifications of the formulae obtained in spherical approximation of wavefronts for the case where offsets under consideration are relatively small. These modifications are performed in two stages.

In the first stage, the time correction formulae (10)–(11) from Part 1 are modified by expanding the radicals entering them in power series and retaining only the first two terms. Practically, this modification does not reduce the area of validity of the spherical approximation.

In the second stage, an additional restriction on offset lengths is introduced. The offsets, satisfying this restriction, are called small ones. The maximum for which the spherical approximation is still valid, lies beyond the area of validity of the formulae found for the small offsets. Thus, a range of the small offsets is essentially less than an interval of validity of the spherical approximation. First, we rewrite the expressions (10)–(11) (from Part 1) for the time correction in the form

$$\Delta\tau_{ij}^{\upsilon} = \left(\sqrt{1 + w_{ij}^{\upsilon}} - 1\right)/\upsilon_0 k_{ij}^{\upsilon} \left(\upsilon = + \text{ or } -\right), \tag{29}$$

where

$$w_{ij}^{\upsilon} = 2\sin\beta_0 k_{ij}^{\upsilon} \Delta x^{\upsilon} + \left(k_{ij}^{\upsilon} \Delta x^{\upsilon}\right)^2 . \tag{30}$$

Expanding the radicals in Eq. (29) in the power series under the conditions

$$(3/48\upsilon_0)\left|\left[\left(w^+\right)^3/k_{ij}^+ + \left(w^-\right)^3/k_{ij}^-\right]\right| \ll T^* , \tag{31}$$

where T^* is a dominant period of the wavepulse, we obtain the following relationship

$$\Delta\tau_{ij} = \left[w^+ + \left(w^+\right)^2/2\right]/\upsilon_0 k_{ij}^+ + \left[w^- + \left(w^-\right)^2/2\right]/\upsilon_0 k_{ij}^- . \tag{32}$$

The last equation for the local time correction has no advantage compared with the initial expression (29) with respect to computations, but the relationship (32) allows to obtain very attractive formulae if a certain additional restriction on the lengths of offsets is made or, in other words, the small offsets are considered. A rough estimate of the small offsets is given by the following inequalities

$$|k_a \Delta x^{\upsilon}| \ll 1 \, (\upsilon = + \text{ or } -) \tag{33}$$

and

$$|2 \sin \beta_0 k_e k_a \Delta x^{+} \Delta x^{-}| \ll (|k_e| + |k_a|)|\Delta x^{\upsilon}|. \tag{34}$$

If a source–receiver distribution satisfies the conditions (33) and (34), then the derived formulae for the parameter γ_{ij}, the curvatures k_{ij}^{υ}, and k_{ij}^{υ} and the time correction can essentially be simplified. Here we are presenting the formulae for reflection shooting while a central trace corresponds to a normally reflected ray.

For the small offsets, Eqs. (17)–(19) for the parameter γ_{ij} and the curvatures k_{ij}^{+} and k_{ij}^{-} can be reduced to the forms

$$\gamma_{ij} = \left(\Delta x_i^{+} - \Delta x_j^{-}\right) / \left(\Delta x_i^{+} + \Delta x_j^{-}\right) \tag{35}$$

and

$$k_{ij}^{+} = \left[(k_{\mathrm{CEE}} + k_{\mathrm{CRE}}) \Delta x_i^{+} + (k_{\mathrm{CEE}} - k_{\mathrm{CRE}}) \Delta x_j^{-}\right] / 2 \Delta x_i^{+}, \tag{36}$$

and

$$k_{ij}^{-} = \left[(k_{\mathrm{CEE}} - k_{\mathrm{CRE}}) \Delta x_i^{+} + (k_{\mathrm{CEE}} + k_{\mathrm{CRE}}) \Delta x_j^{-}\right] / 2 \Delta x_j^{-}. \tag{37}$$

If we introduce the following coordinate system

$$y_{ij} = \left(\Delta x_i^{+} - \Delta x_j^{-}\right) / 2 = \left(x_i^{+} - x_j^{-}\right) / 2 \tag{38}$$

and

$$z_{ij} = \left(\Delta x_i^{+} + \Delta x_j^{-}\right) / 2 = \left(x_i^{+} + x_j^{-}\right) / 2 - x_0 \tag{39}$$

Eqs. (35)–(37) take the forms

$$\gamma_{ij} = \frac{y_{ij}}{z_{ij}}, \; k_{ij}^{+} = \frac{k_{\mathrm{CEE}} z_{ij} + k_{\mathrm{CRE}} y_{ij}}{z_{ij} + y_{ij}}, \; k_{ij}^{-} = \frac{k_{\mathrm{CEE}} z_{ij} - k_{\mathrm{CRE}} y_{ij}}{z_{ij} - y_{ij}}. \tag{40}$$

Substituting the curvatures from equations (40) into the formula (30), grouping the obtained terms according to the power of the offsets y and z, and neglecting the terms of third order and higher, we get the following expression

$$\Delta \tau_{ij} = \left(4 \sin \beta_0 z_{ij} + \cos^2 \beta_0 k_{\mathrm{CEE}} z_{ij}^2 + \cos^2 \beta_0 k_{\mathrm{CRE}} y_{ij}^2\right) / 2 \upsilon_0. \tag{41}$$

Note that all the parameters: υ_0, β_0, k_{CEE}, and k_{CRE} in the last expression relate to the central point $A_0(x_0)$.

Eq. (41) can be written in the form

$$\Delta\tau_{ij} = \Delta\tau_{ij}^{\mathrm{CO}} + \Delta\tau_{ij}^{\mathrm{CMP}}, \tag{42}$$

where

$$\Delta\tau_{ij}^{\mathrm{CO}} = \left(4\sin\beta_0 z_{ij} + \cos^2\beta_0 k_{\mathrm{CEE}} z_{ij}^2\right)/2v_0 \tag{43}$$

and

$$\Delta\tau_{ij}^{\mathrm{CMP}} = \cos^2\beta_0 k_{\mathrm{CRE}} y_{ij}^2/2v_0. \tag{44}$$

Thus, the obtained basic formulae could be interpreted as follows. The NMO for a trace $u(x_i^+, x_j^-, t)$ corresponding to the coordinates y_{ij} and z_{ij} consists of two terms: the first, depending only on a half distance z_{ij} between a middle point $(x_i^+ + x_j^-)/2$ and the fixed central point x_0, and the second term, depending on a half-offset y_{ij} between a receiver x_i^+ and a source x_j^-. It is easy to see that the first term is equal to the CEE correction if $y = 0$ and the second term is the CRE correction if a middle point coincides with the central point. It can be expressed as follows

$$\Delta\tau_{ij}(y = 0) = \Delta\tau_{ij}^{\mathrm{CO}} = \Delta\tau_{ij}^{\mathrm{CEE}}, \tag{45}$$

and

$$\Delta\tau_{ij}(z = x_0) = \Delta\tau_{ij}^{\mathrm{CMP}}\Delta\tau_{ij}^{\mathrm{CRE}}. \tag{46}$$

The given interpretation of the formula (42) is a basis for calling this representation of time correction for the small offsets ''the combined CO and CMP approximation of the NMO''.

4. Analysis of the derived formulae

In this section, we present a brief analysis of the formulae obtained for the curvatures of wavefronts and the time correction for reflection shooting. In order to be accessible to a reader, who is not interested in the proof of the formulae, the consideration begins from a short summary of the expressions needed for the analysis.

Fig. 2 shows a ray tube T_{ij} formed by the central ray $(A_0C_0A_0)$, normally reflected at the point C_0 and a current ray $A_j^-C_{ij}A_i^+$, reflected at the point C_{ij} located nearby the point C_0. These rays correspond to a pair of traces, one of which is a fixed central trace $u(A_0, A_0, t)$. The second trace is recorded, while a source and a receiver are located at the points A_j^- (x_j^-) and A_i^+ (x_i^+) correspondingly. This pair is chosen from a plurality of traces $(i = 0,1,\ldots,m;\ j = 0,1,\ldots,n)$ recorded in a vicinity of the central trace.

The tube T_{ij} has two cross-sections Σ_{ij}^- and Σ_{ij}^+ at the points A_j^- and A_i^+ correspondingly. The front element Σ_{ij}^- moves to the reflector S and the front element Σ_{ij}^+ leaves from S.

The difference in arrival times corresponding to the chosen pair of traces is determined by the formulae (8)–(11) from Part 1

$$\Delta\tau_{ij} = \tau\left(A_j^-C_{ij}A_i^+\right) - \tau(A_0C_0A_0) = \Delta\tau_{ij}^- + \Delta\tau_{ij}^+, \tag{47}$$

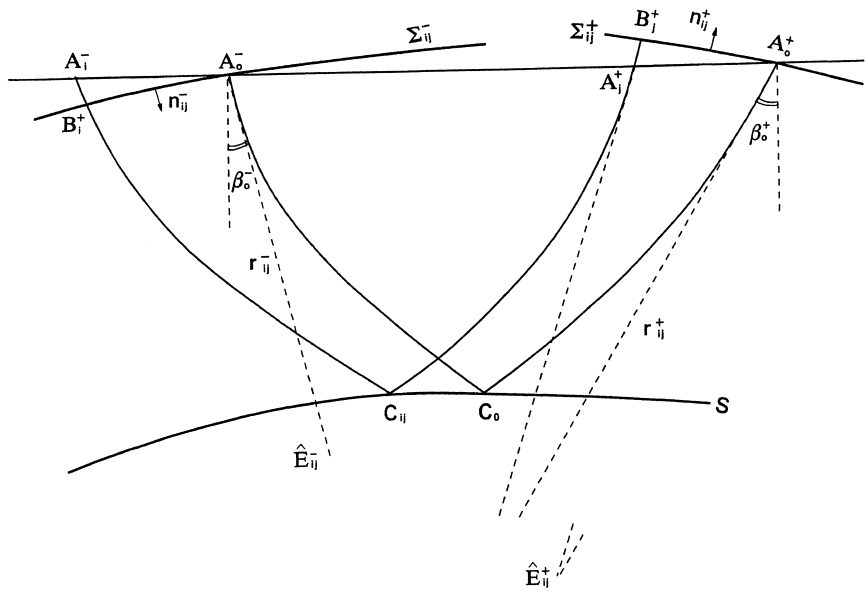

Fig. 2. Ray tube corresponding to a pair of traces (rays). $A_0^- C_0 A_0^+$ is the ray corresponding to the central trace $u(A_0^-, A_0^+, t)$; $A_j^- C_{ij} A_i^+$ is the ray corresponding to the variable trace $u(A_j^-, A_i^+, t)$, the dashed area $(A_0^- C_0 A_0^+ B_i^+ C_{ij} B_j^- A_0^-)$ is the ray tube T_{ij} associated with the pair of the traces $u(A_0^-, A_0^+, t)$ and $u(A_j^-, A_i^+, t)$.

where

$$\Delta\tau_{ij}^- = \left(\left[\left(r_{ij}^-\right)^2 + 2\sin\beta_0 r_{ij}^- \Delta x_j^- + \left(\Delta x_j^-\right)^2\right]^{1/2} - r_{ij}^-\right)/v_0 \tag{48}$$

and

$$\Delta\tau_{ij}^+ = \left(\left[\left(r_{ij}^+\right)^2 + 2\sin\beta_0 r_{ij}^+ \Delta x_i^+ + \left(\Delta x_i^+\right)^2\right]^{1/2} - r_{ij}^+\right)/v_0, \tag{49}$$

where v_0 is a velocity near a seismic line (A_j^-, A_i^+); β_0 is an angle of entry at the point A_0; r_{ij}^v is a radius of the wavefront Σ_{ij}^v ($v = +$ or $-$), and Δ_j^- (Δ_i^+) is an offset of a point A_0^- (A_i^+).

The recorded trace $u(x_i, x_j, t)$ could be time corrected with respect to the central trace $u(x_0, x_0, t)$ with the help of the formulae (48)–(49), if the values of an angle β_0, dual radii (or curvatures) r_{ij}^+ and r_{ij}^- (or k_{ij}^+ and k_{ij}^-) are known or assumed. However, there are difficulties in the direct application of the formulae: the values of r_{ij}^+ and r_{ij}^- change, as a rule, with a change of offsets Δx_j^- and Δx_i^+. Thus, it looks that the time correction depends on a large number of parameters. As it is proved in the paper, this impression is illusive. It is shown in Section 5 of Part 1 that, in fact, the dual curvatures only depend on the three parameters: the angle β_0 and the curvatures r_{CEE} and r_{CRE} of the two basic wavefronts The duel curvature is defined by the expression (39) from Part 1.

$$k_{ij}^+ = \left(k_{\mathrm{CEE}} + \gamma_{ij} k_{\mathrm{CRE}}\right)/\left(1 + \gamma_{ij}\right), \tag{50}$$

and

$$k_{ij}^- = -\left(k_{\mathrm{CEE}} - \gamma_{ij} k_{\mathrm{CRE}}\right)/\left(1 - \gamma_{ij}\right), \tag{51}$$

where the factor γ_{ij} is determined by Eq. (17)

$$\gamma_{ij} = \left(\Delta x_i^+ - \Delta x_j^-\right)/\left(\Delta x_i^+ + \Delta x_j^- - 2\sin\beta_0 k_{\mathrm{CRE}}\Delta x_i^+\Delta x_j^-\right) \tag{52}$$

The two basic wavefronts correspond to the two HI mapping: CEE and CRE (Gelchinsky, 1989; Keydar et al., 1990).

All formulae written above are obtained in a spherical approximation. This means that each wavefront element Σ_{ij}^+ and Σ_{ij}^- is considered as a spherical one (or more precisely, in 2D case as an arc of a circle). A curvature of each element of a wavefront Σ at the end points of a ray is defined by the formulae (50) and (51), depending on the factor γ as a variable, if the basic curvatures k_{CEE} and k_{CRE} are fixed. Use of the last condition (52) means a fixation of the family (or the bundle) of ray tubes surrounding the central ray. We will show now that any chosen value of the factor γ determines a position of the focusing point on the central ray or its continuation.

As it follows from Eq. (16) from Part 1

$$k_\gamma(t) = \left[k_{\mathrm{CEE}}(t) + \sigma_\gamma(t)k_{\mathrm{CRE}}(t)\right]/\left(1 + \sigma_\gamma(t)\right), \tag{53}$$

where

$$\sigma_{\gamma(t)} = \gamma Q_{\mathrm{CRE}}(t)/Q_{\mathrm{CEE}}(t) \tag{54}$$

and $Q(t)$ is a spreading function, a focusing point is determined by the condition

$$1 + \sigma_{\gamma(t)} = 0. \tag{55}$$

The solution of the last equation can be presented in the forms

$$\sigma_{\gamma(t)} = -1,\ \gamma(t) = -Q_{\mathrm{CEE}}(t_\gamma)/Q_{\mathrm{CRE}}(t_\gamma). \tag{56}$$

Thus, the time of propagation t_γ from the initial ray end point A_0 to the focusing point F_γ is determined by Eq. (56). If the condition $0 \le t_\gamma \le t_0$ is met, then a focus is located on the central ray $A_0C_0A_0$ between its end points (Fig. 2). If the inequality $t_\gamma \ge t_0$ (or $t_\gamma \le t_0$) is satisfied, a focus is situated on a continuation of ray behind the receiver A_0^+ (or before the source A_0^-). Using these notations for the ray end point A_0, we would like to underline that it is a double point, where the initial and end points of the ray coincide.

It is worth noting that the developed formalism of the HI multifocusing allows to take into account the presence of a caustic near the central ray. It corresponds to small real values of the CEE or CRE radius in a lighted area or to imaginary values of the radius with small absolute values in a shadow area.

This classification of focusing points is made using a comparison of travel times corresponding to the ray end points and a focus. The approach is convenient for a forward problem consideration. However, this is a nonconstructive approach to the inverse problem, because t_γ is a nonobserved quantity and also could not be used as a parameter. A more amenable classification is based on comparison of dispositions of source and associated receiver with respect to the central point A_0. It is especially useful in data processing.

In Fig. 3, the various ray tube configurations are shown. They are classified according to signs of the source and receiver offsets Δx^- and Δx^+. We see that the fixed ray $A_0C_0A_0$ is accompanied by a bundle of ray tubes of various configurations. This illustration gives a clear geometrical interpreta-

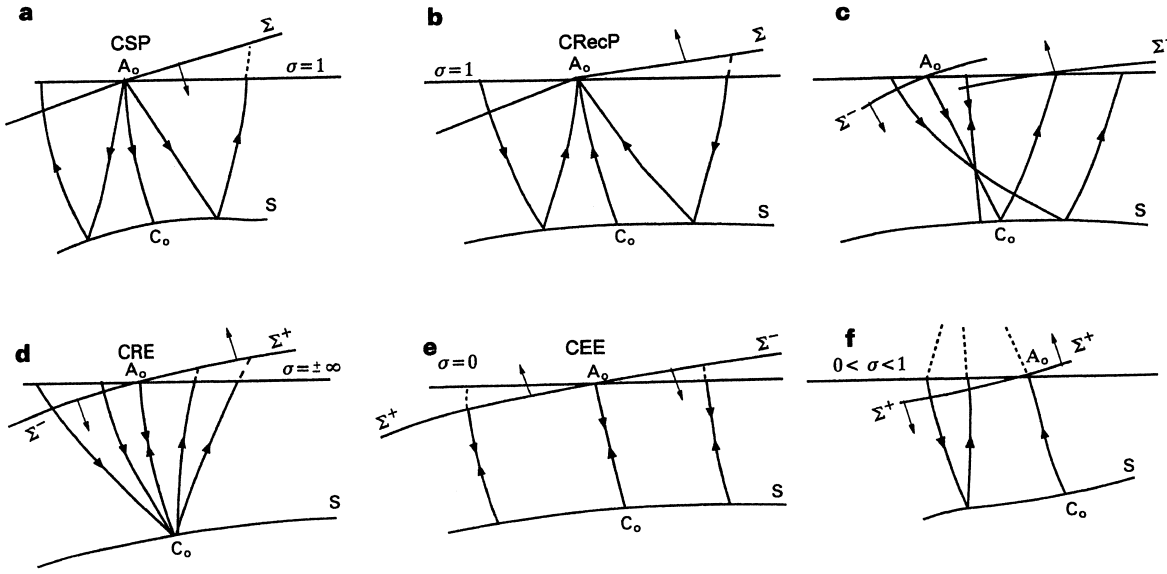

Fig. 3. A set of focusing ray tubes corresponding to the fixed central ray. (a) Focus at the CSP. (b) Focus at the CRecP. (c) Focus at a point located between the source and the reflecting point. (d) Focus at the CRP. (e) Fictitious focus located on the central ray continuation, on the evolute of the reflector (zero offset configuration). (f) Fictitious focus located on the continuation of the central ray beyond the segment connecting the source and the receiver.

tion of the focusing parameter. However, from a practical (data processing) point view, a special diagram, called Multifocusing Stacking Chart, is more convenient.

5. The Multifocusing Stacking Chart

In order to make the consideration of a vicinity of the fixed ray more complete and compact, we are proposing the Multifocusing Stacking Chart (Fig. 4). This is a plane parameterized by the source and receiver coordinate axes x^- and x^+, on which an area of observation is displayed. The area of observation, shown in Fig. 4 in the form of a strip, corresponds to a regular multifold acquisition system with maximum distances between sources and receivers equal to $\Delta x^-_{\max} = \Delta x^+_{\max} = \Delta X_{\max}$. One side of the strip is the zero offset line, another side is a line corresponding to the maximum distance $\Delta x_{\max}$.

The shaded part of the strip is a multifocusing stacking (correlation) area for the fixed central pair $A_0^-(x_0^- = x_0) \Leftrightarrow A_0^+(x_0^+ = x_0)$. The area consists of three parts determined by signs of offsets Δx^- and Δx^+. The central part, defined by the conditions $\Delta x^- \geq 0$ and $\Delta x^+ \geq 0$, is the rectangular triangle with the legs taken equal to the maximum offset $\Delta x_{\max}$. Thus, the triangle hypotenuse *CF* lies on the boundary of the observation area. The border sides *BC* and *GF* of the other two parts, corresponding to the inequalities $\Delta x^- < 0$ and $\Delta x^+ < 0$ or $\Delta x^- > 0$ and $\Delta x^+ > 0$, are defined by the condition $|\Delta x^-| + |\Delta x^+| = \Delta x_{\max}$.

The lines corresponding to the different well-known configurations of source–receiver pairs (like CMP and CRE) are also shown in Fig. 4. By comparing these lines and the multifocusing stacking area, one can define the methods depicted by lines as 1D stacking procedures, and the multifocusing as a 2D stacking procedure.

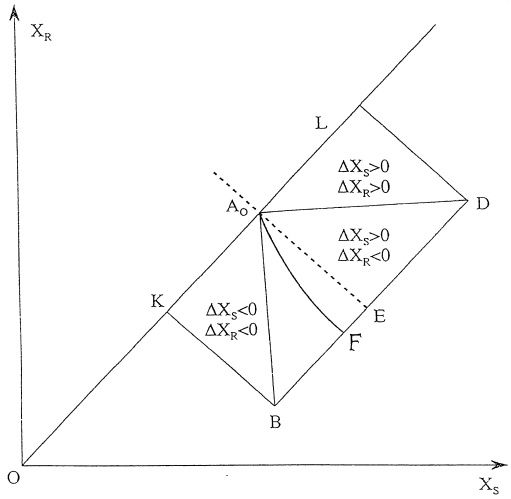

Fig. 4. Multifocusing Stacking Chart. X_s (X_R) is the source (receiver) coordinate axis. OKA_0L is the zero offset (CEE) line, A_0E is the CMP line, A_0F is the CRE line, A_0B is the CSP line, A_0D is the CRecP line, $A_0B = A_0D = \Delta X_{MAX}$ is maximum offset, $BFED$ is the Common Maximum offset line. The quadrangle $KA_0LDEFBK$ is the stacking area.

The number N of traces located in the stacking area $A_0KBEDLA_0$), depends not only on the value Δx_{max}, but also on additional parameters of the acquisition system used. If the CSP seismogram has m traces and the CMP gather consists of n traces, then the number N is equal to

$$N = m \times n. \tag{57}$$

Parameters m and n of modern observation systems are such that N varies from many hundreds to tens of thousands.

If source–receiver pairs are distributed in some other manner, randomly for example, then the number of traces which could be processed using the multifocusing technique is equal to the number of points, with the coordinates located in the stacking area.

Application of the sound time delay formula derived for 2D isotropic media of arbitrary structure in procedures of correlation and stack of a very huge number of traces is a basis of assertion that use of multifocusing will significantly (qualitatively) improve seismic data processing.

It is necessary to note that in Fig. 4, the simple example of stacking area construction is shown. As it follows, the multifocusing area obtained should correspond to the spherical approximation of target wavefronts. In the first place, it refers to the size of this area.

If the size is very small, then a plane approximation is optimal and the front radii could not be found with a good accuracy and reliability. If the size is too large, then a proper front approximation is a nonspherical one and an application of the spherical approximation could lead to instability of determination of multifocusing parameters.

As it was mentioned above, a well-grounded estimation of stacking area size and other parameters can be made in a scope of a general theory of time correction, some elements of which are discussed in the paper by Gelchinsky and Keydar (1993). We intend to devote a special paper to this theory. For the present, we want to draw attention to this problem and propose some simple approximate ways for the cases, where actual value of Δx_{max} clearly does not satisfy conditions for the spherical approximation.

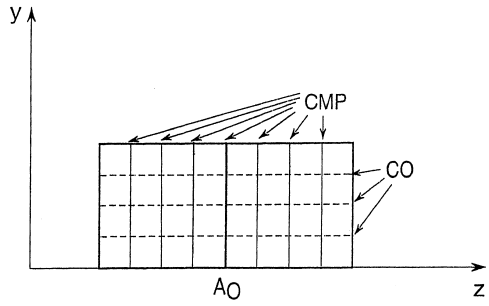

Fig. 5. Multifocusing Stacking Chart for the small offsets (case of combined CMP and CO correlation). While distances A_0D and A_0B (Fig. 4) have small magnitudes, then the CRE line could be approximated as a straight line coinciding with the CMP line. For this case, the most convenient coordinates are: $y=(x_r-x_s)/2$ and $z=(x_r+x_s-z_0)/2$. In this coordinate system, the horizontal CO lines are quasi CEE lines, the vertical CMP lines are quasi CRE lines.

In the cases with a very large length of the maximum offset, a multistep scheme of the multifocusing processing with different sizes of the stacking area (for example, $\Delta x_{\max}/2$ and $\Delta x_{\max}$) may be used. In this scheme, each step has its own optimal interval of the front curvature. A very rough estimation of the interval value could be found using the formulae obtained here for the spherical approximation.

As written above, the single-step procedure with the stacking area shown on Fig. 4 could be considered as optimal one, if values $\Delta x_{\max}$ are not very large.

If maximum offsets are small, i.e., their values met the inequalities (33) and (34), then the proper system of coordinates y_{ij} and z_{ij} is determined by Eqs. (38) and (39)

$$y_{ij}=\left(x_i^+-x_j^-\right)/2,\ \ z_{ij}=\left(x_i^++x_j^-\right)/2. \tag{58}$$

The corresponding Multifocusing Stacking Chart is shown in Fig. 5. In this approximation, the vertical CMP lines can be considered as the CRE lines and the horizontal CO lines as the quasi CEE lines. Thus, multifocusing for the small offsets may be treated as a combination, or better to say, as superposition of the CMP and CO methods.

6. Multifocusing Flow Chart

An algorithm proposed for multifocusing processing exploits a procedure of multichannel correlation (Gelchinsky et al., 1985). We begin the description of the flow chart of multifocusing processing shown on Fig. 6 with the reminder that the presented method corresponds to the kinematic stage of the HI technique. It means that at this stage, all manipulations applied by the construction of the HI apparatus are performed taking into account only geometrical and kinematic properties of wavefields and neglecting their amplitude changes. After determination of the kinematic attributes of body waves, they could be used for finding dynamic characteristics of these waves.

Therefore, in all modifications of the HI technique at the kinematic stage, the first preliminary operation is a normalization of recorded wavefields $u(x_j^-,x_i^+,t)$ (block 4), carried out with the help of their Hilbert transform

$$\hat{u}(x,t)=Hu(x,t)=(1/\pi)\int_{-\infty}^{\infty}\left[u(x,\tau)/(t-\tau)\right]\mathrm{d}\tau. \tag{59}$$

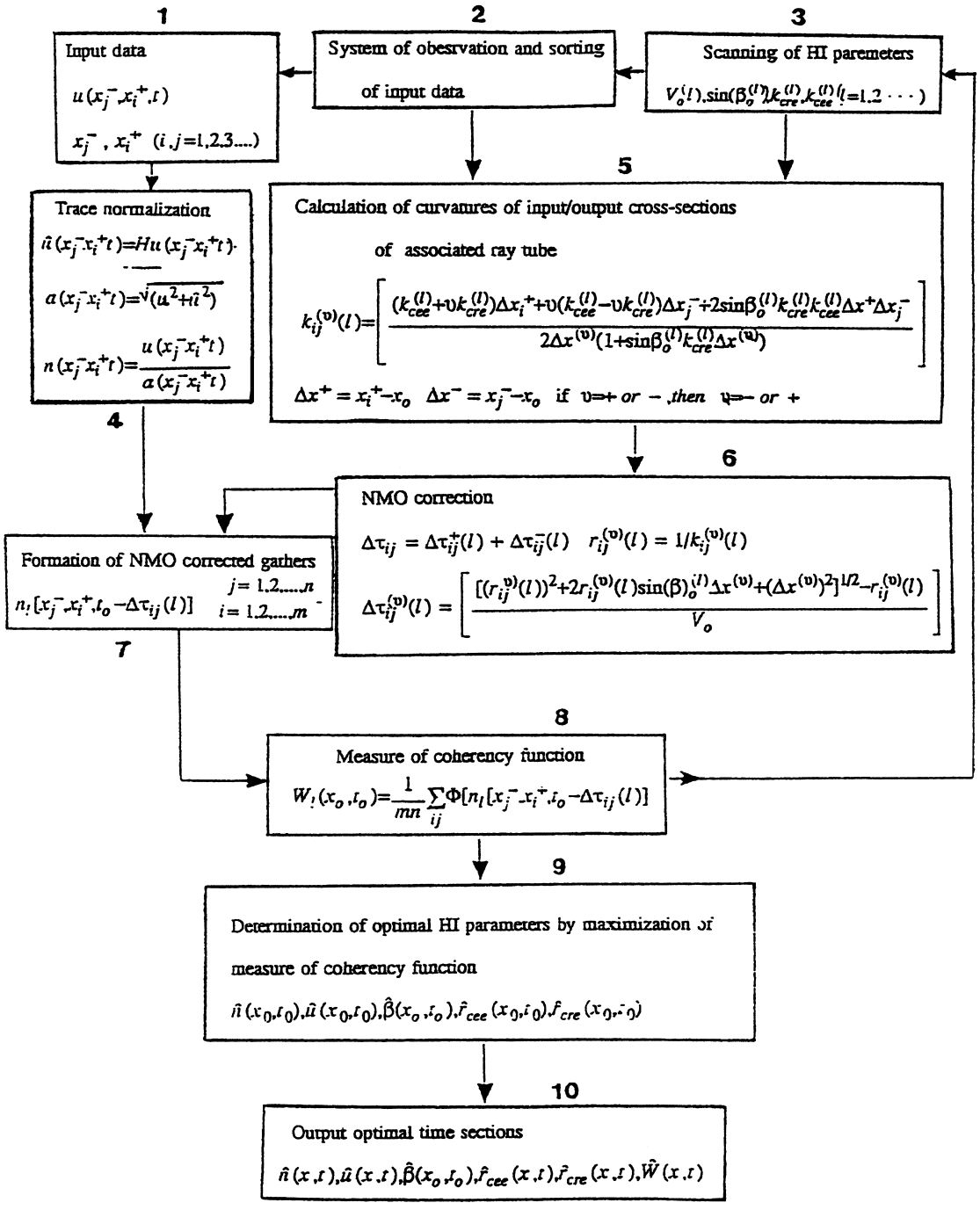

Fig. 6. Multifocusing Flow Chart.

The multifocusing procedure begins to work by fixing the coordinate x_0 of the central trace (block 2) and choosing some l-th combination of values of the HI parameters, sin $\beta_0(l)$, $k_{\mathrm{CRE}}(l)$, $k_{\mathrm{CEE}}(l)$

(block 3). By selecting the parameter values, the program fixes a family of ray tubes surrounding the normal ray, corresponding to the central trace $u(x_0,x_0,t)$. The fixed values of the central coordinate x_0, the parameters and current coordinates of sources x_j^- and receivers x_i^+ are sent to block 5.

Block 5 accomplishes one of the central procedures in the multifocusing processing: juxtaposition of a set of coordinates of source–receiver pairs x_j^- and x_i^+ to a bundle of ray tubes T_{ij} associated with the central ray A_0A_0 and having the curvatures of dual cross-sections $k_{ij}^-(l)$ and $k_{ij}^+(l)$ correspondingly.

The values of the computed curvatures $k_{ij}^-(l)$ and $k_{ij}^+(l)$ are sent from block 5 to block 6 for calculation of time correction $\Delta\tau_{ij}(l)$. They are sent to block 7 which corrects normalized traces entering from block 4. A gather of the corrected traces $n[x_j^-,x_j^+,t-\Delta\tau_{ij}(l)]$ is sent from block 7 to block 8 for calculation of a fixed coherency function (e.g., semblance) $W_l(x_0,t)$ corresponding to the l-th chosen combination of the multifocusing parameters.

Block 7 transmits the coherency function to the optimization block 8, which produces a command to block 3 to change the combination of the parameters and a new circle of the coherency function calculation is repeated. As a result of such circles of repetitions, a set of coherency functions comes into in the optimization block, which finds optimal parameter values $\hat{\beta}_0(x_0,t_0)$, $\hat{r}_{\mathrm{CRE}}(x_0,t_0)$, $\hat{r}_{\mathrm{CEE}}(x_0,t_0)$ corresponding to $\max_l W_l(x_0,t_0)=\hat{W}(x_0,t_0)$ at each moment t_0 and each central coordinate x_0. After the determination of the optimal parameters, the optimally stacked traces $\hat{n}(x_0,t_0)$ and $\hat{u}(x_0,t_0)$ are also calculated.

Output is the ensemble of time sections presenting the averaged dynamic attributes: stacked wavefields $\hat{u}(x_0,t_0)$, $\hat{n}(x_0,t_0)$, and $\hat{W}(x,t_0)$ and the optimal kinematic attributes: angle (anglegram), CEE and CRE radii (CEE and CRE radiusgram), as 2D functions of the coordinate of central point x_0 and the time t_0.

7. Discussion and conclusions

The presented method may be considered in various aspects. The first arising question, naturally, concerns practical aspects of the method, or in more concrete terms, the results of its testing on real or synthetic data. The first results of the applications of the multifocusing technique are presented in the works by Berkovitch (1995) and Berkovitch et al. (1996). We prepared the paper summarizing the competitive studies of salt dome flanks by alternative processing techniques including conventional, CEE, scattering-diffraction waves, and multifocusing methods (Gelchinsky et al., 1992, 1993; Berkovitch et al., 1996). The paper contains the analysis of the obtained results and certain recommendations.

Here we would like to touch upon certain general aspects of the work. The two parts of the present paper form the basis of multifocusing theory. We would like to attract the attention to the fact, that this 2D version of the theory is constructed with minimum of premises. Only one premise is fundamental and necessary: it is the existence of a body wave on a recorded central trace. Other assumptions, such as the sphericity of wavefront's elements, a homogeneity of medium nearby sources and receivers lines, etc. have a technical character and could be removed within the scope of the theory. Making use of such a weak restriction as the existence of a body wave on a central trace (if it is a restriction at all), we have to create the theory of a very general nature. We did it, developing the theory based on description of a geometry of the infinite family of dual cross-sections (wavefronts) at sources and receivers locations of all possible ray tubes, surrounding the central ray,

corresponding to the central trace. This basis of the theory allows us to consider very general situations: media of arbitrary structure, acquisition systems situated on two lines in the vertical plane and so on.

From another side, the HI multifocusing approach to correction, correlation and stacking multifold data involves a new approach to traditional problems, for example, the computation of wave kinematics. As we see, a global time field, corresponding to multifold data recorded on two lines is determined by the calculation of travel times, dual curvatures for two fundamental (e.g., CEE and CRE) ray tubes along a set of selected central rays (see also Hubral, 1983; Tygel et al., 1992; Schleicher et al., 1993). We called these quantities as the kinematic attributes of a pseudo-plane wave propagating along the central rays between end points, situated on the two fixed lines. From this point of view, the presented multifocusing procedure can be considered as a digital apparatus transforming multifold total seismic fields into an ensemble of images of the kinematic and dynamic attributes of a recorded pseudo-plane wave (like anglegrams, radiusgrams of two basic types, stacked normalized traces, and stacked wavefields).

The kinematic attributes of a pseudo-plane wave can be used in various directions. As it was said in the first part of the paper, they together with wavefields corrected for spreading function are input in the new type of migration along central rays. In other application, the kinematic attributes may be used as input in algorithms of inverse kinematic problem solution. Their simplest versions are proposed by Berkovitch and Gelchinsky (1989), Berkovitch et al. (1991), and Keydar et al. (1995).

The presented multifocusing algorithm could also be considered as the first kinematic step in construction of method of studies of body wave dynamics. A local asymptotic nature of any body wave determines a way of calculating (in forward modeling) or studying (in processing and inverse problem) its dynamics, which could only be carried out on a basis of constructed kinematic skeleton. In the considered case, amplitudes and other dynamics attributes can be investigated along travel time curves, found on the first step.

A novel direction in kinematic attributes application is connected with topological properties of the HI technique (Gelchinsky, 1989; Gelchinsky and Keydar, 2000). Propagation of a reflected wave near a fixed line is considered as a topological mapping of a corresponding reflector in its CEE and CRE images. Because these images are homeomorphisms of the reflector, all their characteristic points are imaged in reflector's characteristic points (like maxima, minima, inflection and angle points, wedges, etc.). Therefore, the patterns of characteristic points of the images (or the HI portraits) represent the original's (reflector's) portraits (Gelchinsky et al., 1995). According to modern concepts in physics and mathematics (theory of catastrophes or singularities of differentiable mappings, see Gilmor, 1981; Arnold et al., 1988; Arnold, 1992), patterns of singularities (characteristic points) found by a mathematical description of some phenomena (objects) give an essential information concerning its specific features. Analogous situation should be expected in geology and geophysics. For example, the tracing of a closure line is a very important procedure of mapping geological structures containing hydrocarbons. From a geometrical point of view, the closure line is a characteristic line of a structure under consideration: this line passes through inflection points.

It is worth noting that the characteristic points are detected in the HI images, which are obtained with the minimum assumption as the results of correlation and stacking of many hundreds and thousands traces. Thus, their determination is accomplished in a more accurate and reliable way than that could be done at a migrated section or on a seismic model after solving an inverse problem. We had dwelled at some length on this issue, because, to our knowledge, the use of topological images for discovery and studies of structural singularities is a completely new approach in geophysics. We believe that this approach will bring fruitful results in geophysical practice and theory.

It is also relevant to mention, that the first attempts to detect characteristic points at parameter curves constructed from anglegrams and radiusgrams turned out to be very successful (Keydar et al., 1990; Gelchinsky et al., 1992, 1993; Berkovitch et al., 1996). In the majority of cases, the characteristical points are found clearly and certainly. Their disposition of angle and radius curves very often are consistent and correspond to the theory. Besides, the direct HI method of determination of the angle points of studied structures was proposed (Gelchinsky et al., 1995). The locations of the angle points on the time section are accomplished directly from recorded seismograms as a result of the correlation procedure. This method is the modification of multifocusing technique created on the basis of the asymptotic formulae for wavefields formed by the angle points.

Acknowledgements

The authors thank Dr. Boris Gurevitch for the useful discussion and the valuable remarks.

Appendix A. Derivation of formula for coefficient of asymmetry α

In Section 1, the expression (9)

$$2\alpha = -\left(\frac{\cos\beta_0^-}{\cos\beta_0^+}\right)\frac{\mathrm{d}}{\mathrm{d}x^+}\left(\frac{\cos\beta^+}{\cos\beta^-}\right) \tag{A-1}$$

was given as the definition of the coefficient α of Eq. (8) for a source–receiver distribution. Here the derivation of the formula (10) used in this paper for the coefficient α from the expression (A-1) is presented.

We start from the relationship

$$\cos\beta^{\upsilon} = -\upsilon(\boldsymbol{n}^{\upsilon}\boldsymbol{N})\ (\upsilon = +\ \text{or}\ -) \tag{A-2}$$

obviously from the geometrical point of view (Fig. 1). Differentiating Eq. (A-2) with respect to x^{υ}, we obtain

$$\frac{\mathrm{d}\cos\beta_0^{\upsilon}}{\mathrm{d}x^{\upsilon}} = (\upsilon)\frac{\sin\beta_0^{\upsilon}\cos\beta_0^{\upsilon}}{r_0^{\upsilon}}, \tag{A-3}$$

if the plain seismic lines ($\mathbf{N} = \mathbf{const}$) are considered. By derivation of the expression (A-3), the well-known formula is used

$$\mathrm{d}\boldsymbol{n}/\mathrm{d}s = \boldsymbol{t}/r, \tag{A-4}$$

where **t** is the unit vector tangent to the wavefront which was applied.Substituting the expression $\mathrm{d}x^-/\mathrm{d}x^+ = (1-2b)(\cos\beta_0^+/\cos\beta_0^-)$ following from Eq. (7) in the formula (A-3) (by $\upsilon = -$), we obtain the relationship

$$\frac{\mathrm{d}\cos\beta_0^-}{\mathrm{d}x^+} = -\sin\beta_0^-\cos\beta_0^+. \tag{A-5}$$

Substituting the expressions (A-3) and (A-5) found for the derivatives of $\cos\beta_0^{\upsilon}$, in the relationship

$$\frac{\mathrm{d}}{\mathrm{d}x^+}\left(\frac{\cos\beta^+}{\cos\beta^-}\right) = \frac{1}{\cos\beta^-}\frac{\mathrm{d}\cos\beta^+}{\mathrm{d}x^+} - \frac{\cos\beta^+}{\cos^2\beta^-}\frac{\mathrm{d}\cos\beta^-}{\mathrm{d}x^+}, \tag{A-6}$$

we obtain

$$\frac{\mathrm{d}}{\mathrm{d}x^+}\left(\frac{\cos\beta_0^+}{\cos\beta_0^-}\right)=\frac{\sin\beta_0^+\cos\beta_0^+}{\cos\beta_0^-}k_0^+ + \frac{\sin\beta_0^-\cos^2\beta_0^+}{\cos^2\beta_0^-}(1-2b)k_0^-. \tag{A-7}$$

After substitution of the last expression in the relationship (A-1), the formula

$$2\alpha = -\left[\sin\beta_0^+\cos\beta_0^- k_0^+ + (1-2b)\sin\beta_0^-\cos\beta_0^+ k_0^-\right]/\cos\beta_0^- \tag{A-8}$$

is found.

Taking into account the formula (6): $\gamma = b/(1-b)$, we transform Eq. (20) from Part 1 to the forms

$$k_0^+ = (1-b)k_e^+ + bk_a^+,\ k_0^- = \left[(1-b)k_e^- - bk_a^-\right]/(1-2b), \tag{A-9}$$

substituting them in the expression (A-8); the desirable formula (10) is obtained.

$$2\alpha = -\frac{\sin\beta_0^+\cos\beta_0^-\left[(1-b)k_e^+ + bk_a^+\right] + \sin\beta_0^-\cos\beta_0^+\left[(1-b)k_e^- - bk_a^-\right]}{\cos\beta_0^-}. \tag{A-10}$$

References

Arnold, V.I., 1992. Catastrophe Theory, 3rd edn. Springer.

Arnold, V.I., Varchenko, S.M., Gusein-Zade, S.M., 1988. Singularities of Differentiable Mappings. Birkhauser.

Berkovitch, A., 1995. The multifocusing method for homeomorphic imaging and stacking of seismic data, PhD Thesis, Tel-Aviv University.

Berkovitch, A., Gelchinsky, B., 1989. Inverse of common reflecting element data, 59th Ann. Intern. Mtg., Soc. Exp. Geophys., Expanded Abstracts, pp. 1250–1253.

Berkovitch, A., Gelchinsky, B., Keydar, S., Shtivelman, V., 1991. Inversion of combined data of the CRE and CEE imaging (Stacks), 53rd Mtg. and Tech. Exh. AO-23.

Berkovitch, A., Keydar, S., Helle, H.B., Gelchinsky, B., 1996, A comparative study of salt dome flanks by alternative processing techniques, 58th Conf. and Tech. Exh., PO-84.

Gelchinsky, B., 1989, Homeomorphic imaging in processing of seismic data (fundamentals and schemes), 59th Ann. Intern. Mtg., Soc. Exp. Geophys., Expanded Abstracts, pp. 883–888.

Gelchinsky, B., Keydar, S., 1993a. Basic HI formulae of general theory of local time correction, 63rd Ann. Intern. Mtg., Soc. Exp. Geophys., Expanded Abstracts, pp. 1145–1447.

Gelchinsky, B., Keydar, B., 2000. Homeomorphic Imaging: Theory and Practice, the present issue.

Gelchinsky, B., Landa, E., Shtivelman, V., 1985. Algorithms of phase and group correlation. Geophysics 50, 596–608.

Gelchinsky, B., Keydar, S., Helle, H., 1992. Structural imaging of a salt dome by HI methods, Vol. 59, Sesmo-Series. Bergen University, pp. 1–59.

Gelchinsky, B., Keydar, S., Helle, H., 1993. Studying of salt dome by homeomorphic technique — a case of history, 55th EAEG Conf. and Tech. Exh., Extended Abstracts, PO-64.

Gelchinsky, B., Hanyga, A., Berkovitch, A., Keydar, S., 1995. Determination of wedge points by high resolution homeomorphic imaging method, 57th EAEG Conf. and Tech. Exh., Extended Abstracts, BO-39.

Gilmor, R., 1981. Catastrophe Theory for Scientists and Engineers. Wiley.

Hubral, P., 1983. Computing true amplitude reflections in a lateraly inhomogeneous Earth. Geophysics 48, 1051–1062.

Keydar, S., Gelchinsky, B., Shtivelman, V., Berkovich, A., 1990. The Common Evolute Element (CEE) stack method (zero-offset stack), 60th Ann. Intern. Mtg., Soc. Exp. Geophys., Expanded Abstracts, pp. 1911–1913.

Keydar, S., Edry, Berkovitch, A., Gelchinsky, B., 1995. Construction of kinematic seismic model by homeomorphic imaging method, 57th EAEG Conf. and Tech. Exh., Extended Abstracts, BO-86.

Schleicher, J., Tygel, M., Hubral, P., 1993. 3D true-amplitude finite-offset migration. Geophysics 58, 1112–1126.

Tygel, M., Schleicher, J., Hubral, P., 1992. Geometrical-spreading correction of offset reflections in a lateraly inhomogeneous Earth. Geophysics 57, 1054–1063.